Proceedings of IMECE2007
2007 ASME International Mechanical Engineering Congress and Exposition
November 11-15, 2007, Seattle, Washington, USA

IMECE2007-42106

DESIGN OF A MAGNETIC FIELD-BASED MULTI DEGREE-OF-FREEDOM ORIENTATION SENSOR USING THE DISTRBUTED-MULTIPLE-POLE MODEL

Kok-Meng Lee
Professor, Woodruff School of Mechanical Engineering
Georgia Institute of Technology
Atlanta, GA 30332-0405

Hungsun Son
Ph. D. Candidate, Woodruff School of Mechanical Engineering
Georgia Institute of Technology
Atlanta, GA 30332-0405

ABSTRACT

Precision control of a tiltable spinning shaft requires real-time measurement of the inclination. Conventional single-axis encoders, though capable of providing high-resolution (linear or angular) measurements, rely on mechanical linkages (that often introduce frictions, backlashes, and singularities) to constrain the device so that the three-DOF motion can be deduced from the individual orthogonal measurements. Vision-based sensors, which have the attractive features of being non-contact, are limited to low speed measurements. We present here an efficient method for designing a magnetic field-based orientation sensor for devices where orientation control of a rotating shaft under the influence of a magnetic field is required. The ability to characterize the magnetic fields and forces in addition to orientation sensing can offer a number of advantages in real-time computation and control.

INTRODUCTION

Precision machine tools, automated cutting of deformable food products (such as poultry, meat and fish), gyroscopes and mobile vehicles (such as car wheels [1] [2], propellers for boats, helicopter or underwater vehicle) require orientation measurement and control of a rotating shaft. The use of single-axis encoders for measuring 3-DOF motions often requires a mechanism to constrain the device so that the 3-DOF motion can be deduced from the three individual orthogonal measurements. The desire to eliminate the constraining mechanism, which often introduces significant friction and inertia, has motivated Lee and his co-workers to develop alternative image-based methods for measuring the 3-DOF orientation of a spherical body [3] [4] [5]. Image-based sensors, which have the attractive features of being non-contact, are limited to low speed measurements. For devices such as a PM-based spherical wheel motor (SWM) [6] or a high-speed spindle, the ability to measure magnetic fields and forces in real-time can broadened the applications of a SWM.

Magnetic sensors are widely available at low cost due to the rapid advancement of semiconductor fabrication technology; a review of commonly used magnetic field sensing techniques can be found in [7]. For example, the Hall-effect sensors which can measure either a constant or a varying flux possess both small size and CMOS compatibility [8]. The frequency limitation is about 1MHz. They are light and about $0.1in^2$. Their power requirement is between 0.1 and 0.2W, and they can be operated over an extremely wide temperature range from 200°C to near absolute zero (-273°C). The advantages of Hall-effect sensors, although they are widely availability at low-cost, are seldom exploited for real-time multi-DOF motion control applications because of complicated field analysis involved in their design. Existing techniques for analyzing electromagnetic fields and for real-time control of a multi-DOF PM-based actuator rely primarily on two approaches; namely, numerical methods or lumped-parameter analyses with some form of magnetic equivalent circuits. These approaches have difficulties in achieving both accuracy and low computation time simultaneously.

Recently, Lee *et al*. developed a new modeling method to derive closed-form solutions for characterizing the magnetic fields of a PM [9] or an electromagnet [10] by using multiple distributed poles (DMP) for designing a PM-based device. While a single dipole has been a widely used model to analyze the magnetic field at a sufficiently large distance for applications [11] [12], it generally gives a poor approximation when the length scale of the field is very small. The DMP method inherits many advantages of the dipole model originally conceptualized in the context of physics, but provides an effective means to account for the shape and magnetization of the physical magnet. This paper extends the DMP method developed in [9] deriving the inverse solution of the DMP model for the design of a multi-DOF orientation sensor using magnetic sensors.

The remaining paper offers the following:

1. We present a method for designing a magnetic field-based orientation sensor using an assembly of magnetic sensors (such as Hall-effect) along with one or more high-coercive permanent magnets which are designed for both actuation and orientation sensing.
2. We extend the distributed multi-pole (DMP) modeling method for deriving a PM-based orientation sensor. Unlike other field calculation methods (such as FEM), the DMP models can be computed in real-time for motion estimation. Once the magnetic fields are obtained, the forces and torques

on the PM assembly can also be computed from the surface integration in terms of a Maxwell stress tensor.

3. A design analysis detailing the effects of key design parameters on the performance of the magnetic field-based orientation sensor is given. While developed in the context of a spherical motor, the modeling techniques presented in this paper are applicable to other PM-based actuator and sensing systems.

MAGNETIC FIELD FOR SENSOR FORMULATION

Figure 1 defines the coordinate systems used in formulating the PM-based orientation measuring system, where a and ℓ are the radius and length of the cylindrical PM; and $\mathbf{M}$ is its magnetization.

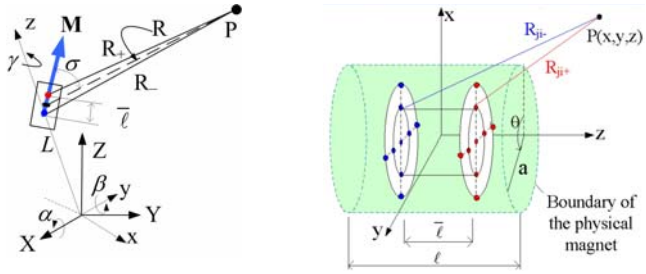

(a) moving PM (b) DMP model

Fig. 1 Coordinate system illustrating the DMP model

In Fig. 1(a), the PM moves with the rotating *xyz* coordinate frame; and the distance L that describes the center of the PM is known by design. The location and orientation with respect to the XYZ reference frame are described by the coordinate transformation:

$$\mathbf{P} = \Gamma(\mathbf{q})\mathbf{p} \tag{1}$$

where $\mathbf{q} = [\alpha \ \beta \ \gamma]^{\mathrm{T}}$ is the orientation vector in terms of xyz Euler angles. The unit vector $\hat{\mathbf{z}}$ can be expressed in the XYZ frame as

$$\hat{\mathbf{z}} = \begin{bmatrix} \sin\beta\cos\alpha & -\sin\alpha & \cos\beta\cos\alpha \end{bmatrix}^{\mathrm{T}} \tag{2}$$

The PM is modeled analytically [9] using k circular loops (each with radius $\bar{a}_j$, j = 0… k) of n dipoles (strength m_j) in parallel to its magnetization vector as illustrated in Fig. 1(b). We define here a *dipole* as a pair of source and sink separated by a distance $\bar{\ell}$ ($0 < \bar{\ell} < \ell$). The coordinates of the source and sink, $\mathbf{p}_{ji+}$ and $\mathbf{p}_{ji-}$ respectively, are known constants in *xyz* frame. In Fig. 1(b), R_{ji+} and R_{ji-} are the distances from the i^{th} dipole in j^{th} loop, to the sensor located at $\mathbf{P}$. In XYZ reference frame,

$$\mathbf{B} = \frac{\mu_o}{4\pi}\sum_{j=0}^{k} m_j \sum_{i=1}^{n_k}\left(\frac{\mathbf{a}_{Rji+}}{R_{ji+}^2} - \frac{\mathbf{a}_{Rji-}}{R_{ji-}^2}\right) \tag{3}$$

where

$$R_{ji\pm} = \left|\mathbf{P} - \mathbf{P}_{ji\pm}\right|; \tag{3a}$$

$$\mathbf{P}_{ji\pm} = \Gamma(\mathbf{q})\mathbf{p}_{ji\pm}; \tag{3b}$$

$$\mathbf{p}_{ji\pm} = \begin{bmatrix} x_{ji} & y_{ji} & z_{ji\pm} \end{bmatrix}^{\mathrm{T}}; \tag{3c}$$

and

$$\frac{\mathbf{a}_{Rji\pm}}{R_{ji\pm}^2} = -\frac{\mathbf{P} - \Gamma(\mathbf{q})\mathbf{p}_{ji\pm}}{\left|\mathbf{P} - \Gamma(\mathbf{q})\mathbf{p}_{ji\pm}\right|^3} \tag{3d}$$

Equation (3) provides a means to determine the unknown orientation $\mathbf{q}(\alpha, \beta, \gamma)$ from the magnetic flux density $\mathbf{B}$ using field-based sensors. However, the unknown orientation $\mathbf{q}$ must be solved implicitly from (1) and (3).

As will be shown, the inverse problem can be solved from $B_{X\pm}$ and $B_{Y\pm}$ measured using two sensor-pairs located respectively at

$$\mathbf{S}_{1\pm} = \begin{bmatrix} \pm S & 0 & Z_s \end{bmatrix}^{\mathrm{T}} \text{ and } \mathbf{S}_{2\pm} = \begin{bmatrix} 0 & \pm S & Z_s \end{bmatrix}^{\mathrm{T}} \tag{4a,b}$$

where the subscript $i\pm$ denotes the i^{th} sensor pair.

Illustrative Example 1

To illustrate the use of the DMP model (3) for designing an orientation sensor, we make the following simplifications for clarity in explanation:

(a) The sensors are located such that $R >> \bar{\ell}, \bar{a}$.

(b) Sensor are oriented such that $\sigma \approx 90°$; $\bar{\ell}\cos\sigma / R \ll 1$.

From Assumption (a),

$$R_{\pm}^{-3} \approx \left(R \mp \bar{\ell}\cos\sigma/2\right)^{-3} \approx R^{-3}\left[1 \pm 3\bar{\ell}\cos\sigma/(2R)\right] \tag{5}$$

This reduces the expression for $\mathbf{B}$ to

$$\mathbf{B} \approx \frac{\mu_o}{4\pi R^3}\left(1 - \frac{3\bar{\ell}\cos\sigma}{2R}\right)\sum_{j=0}^{k}\sum_{i=1}^{n_k} m_j\left(\mathbf{P}_{\mathbf{ji+}} - \mathbf{P}_{\mathbf{ji-}}\right) \tag{6}$$

As shown in Fig. 1(a), $\cos\sigma = \mathbf{M}\bullet\mathbf{R} / \left(\left|\mathbf{M}\right|\left|\mathbf{R}\right|\right)$. In (6), $\mathbf{P}_{\mathbf{ji+}} - \mathbf{P}_{\mathbf{ji-}}$ is the vector of length $\bar{\ell}$ in XYZ frame.

For the sensor locations defined in (4a,b), Assumption (b) implies

$$\rho_X = \frac{B_{X+}}{B_{X-}} = \frac{R_{1-}^3}{R_{1+}^3} \text{ and } \rho_Y = \frac{B_{Y+}}{B_{Y-}} = \frac{R_{2-}^3}{R_{2+}^3} \tag{7}$$

where the sensor location $R_{i\pm} = \left|\mathbf{S}_{i\pm} - \mathbf{P}_{\mathbf{m}}\right|$ is given by

$$R_{1\pm}^2 = \left(\pm S - X_m\right)^2 + Y_m^2 + \left(Z_s - Z_m\right)^2 \tag{8a}$$

$$R_{2\pm}^2 = X_m^2 + \left(\pm S - Y_m\right)^2 + \left(Z_s - Z_m\right)^2 \tag{8b}$$

In (8a, b), $\mathbf{P}_{\mathbf{m}} = \begin{bmatrix} X_m & Y_m & Z_m \end{bmatrix}^{\mathrm{T}}$ defines the center of the PM;

$$X_m^2 + Y_m^2 + Z_m^2 = L^2 \tag{9}$$

Equations (7) to (9), which implicitly relate $\mathbf{B}$ to $\hat{\mathbf{z}}$ through R and σ, can be used to solve X_m, Y_m and Z_m in closed form. Expanding (8a,b) with (9),

$$R_{1+}^2\left(\rho_X^{2/3} - 1\right) = 4X_m S \tag{10a}$$

$$R_{1+}^2\left(\rho_X^{2/3} + 1\right) = 2\left(S^2 + Z_s^2 - 2Z_m Z_s + L^2\right) \tag{10b}$$

$$R_{2+}^2\left(\rho_Y^{2/3} - 1\right) = 4Y_m S \tag{10c}$$

$$R_{2+}^2\left(\rho_Y^{2/3} + 1\right) = 2\left(S^2 + Z_s^2 - 2Z_m Z_s + L^2\right) \tag{10d}$$

Eliminating R_{1+}^2 from (10a) and (10b) and R_{2+}^2 from (10c) and (10d) leads to (11a) and (11b) respectively:

$$X_m = m_X\left(hZ_m - H\right);\ Y_m = m_Y\left(hZ_m - H\right) \tag{11a,b}$$

where $m_X = \left(1 - \rho_X^{2/3}\right)/\left(1 + \rho_X^{2/3}\right)$; $m_Y = \left(1 - \rho_Y^{2/3}\right)/\left(1 + \rho_Y^{2/3}\right)$;

$h = Z_s / S$; and $H = S\left(1 + h^2 + L^2/S^2\right)/2$.

From (9) and (11a,b),

$$Z_m = \frac{hH}{1+\left(m_X^2+m_Y^2\right)h^2}\left\{1 \pm \sqrt{1+\left[1+\left(m_X^2+m_Y^2\right)h^2\right]\left(\frac{L^2}{H^2}-\frac{1}{h^2}\right)}\right\} \quad (11c)$$

In (11a, b, c), the parameters (m_X and m_Y) are measured quantities; and h and H are constants characterizing the placement of the sensor pairs. Once $\mathbf{P_m} = \begin{bmatrix} X_m & Y_m & Z_m \end{bmatrix}^{\mathrm{T}}$ is known, the orientation (α, β) can be solved from the unit vector $\hat{\mathbf{z}}$ in (2).

The above example illustrates how the shaft inclination can be determined from two orthogonal magnetic sensor-pairs. While the assumption that the PM can be approximated as a single dipole permits the orientation (α, β) to be solved in closed form, it has some practical limitations where R and $\overline{\ell}$ are in the same order.

MAGNETIC ORIENTATION SENSOR

To allow for a broader application of the magnetic sensors for measuring the orientation of a three-DOF actuator in real time, two different alternatives which relax the single dipole assumption are derived in this section; incremental and absolute orientation.

A. Incremental Orientation

The common approach to reduce (3) for a real-time application is to compute the incremental change in orientation,

$$\hat{\mathbf{q}} = \mathbf{q}_{k+1} - \mathbf{q}_k \quad (12)$$

such that the orientation $\mathbf{q}_{k+1}$ at $(k+1)^{\text{th}}$ time step is computed from its previous step $\mathbf{q}_k$ based on the perturbation model of (3):

$$[\mathbf{A}]\hat{\mathbf{q}} = \mathbf{b} \quad (13)$$

where $\hat{\mathbf{q}} = \begin{bmatrix} \hat{\alpha} & \hat{\beta} & \hat{\gamma} \end{bmatrix}^{\mathrm{T}}$; $\mathbf{b} = \left[\mathbf{B}(\mathbf{q}_{k+1}) - \mathbf{B}(\mathbf{q}_k)\right]$ (13a,b)

and $$[\mathbf{A}] = \left[\frac{\partial \mathbf{B}}{\partial \alpha} \quad \frac{\partial \mathbf{B}}{\partial \beta} \quad \frac{\partial \mathbf{B}}{\partial \gamma}\right]_{\mathbf{q}=\mathbf{q}_k} \in \mathbb{R}^{j\times 3} \quad (13c)$$

For a sensor located $\mathbf{P}$,

$$\frac{\partial \mathbf{B}}{\partial q} = -\frac{\mu_o}{4\pi}\sum_{j=0}^{k} m_j \sum_{i=1}^{n_k} \frac{\partial}{\partial q}\left(\frac{\mathbf{R_{ji+}}}{\left|\mathbf{R_{ji+}}\right|^3} - \frac{\mathbf{R_{ji+}}}{\left|\mathbf{R_{ji+}}\right|^3}\right) \quad (14)$$

where q denotes α, β or γ; and $\mathbf{R_{ji\pm}} = \mathbf{P} - \mathbf{P_{ji\pm}}$. The partial derivative in (15) is given by

$$\frac{\partial}{\partial q}\left(\frac{\mathbf{R_{ji\pm}}}{\left|\mathbf{R_{ji\pm}}\right|^3}\right) = -\frac{1}{\left|\mathbf{R_{ji\pm}}\right|^3}\frac{\partial \mathbf{P_{ji\pm}}}{\partial q} + \left(3\left[\mathbf{R_{ji\pm}}\right]^{\mathrm{T}}\frac{\partial \mathbf{P_{ji\pm}}}{\partial q}\right)\frac{\mathbf{R_{ji\pm}}}{\left|\mathbf{R_{ji\pm}}\right|} \quad (15a)$$

where $$\partial \mathbf{P}_{ji\pm} / \partial q = \nabla\left[\Gamma(\mathbf{q})\mathbf{p}_{ji\pm}\right] \quad (15b)$$

and $\nabla = \partial/\partial\alpha + \partial/\partial\beta + \partial/\partial\gamma$.

Once [**A**] is computed, the orientation can be updated:

$$\mathbf{q}_{k+1} = \mathbf{q}_k + \left(\left[\mathbf{A}\right]^{\mathrm{T}}\left[\mathbf{A}\right]\right)^{-1}\left[\mathbf{A}\right]^{\mathrm{T}}\mathbf{b} \quad (16)$$

Equations (3) and (16) provide a general formulation of a field-based sensor for incremental orientation measurement in real-time computation.

B. Absolute Orientation with Polynomial Approximation

Another alternative to determine the absolute orientation in real time is to express the measured magnetic field density $\hat{B}$ of the sensor as a polynomial function and solve the inverse problem (of computing the rotor orientation from the measured magnetic field). The method has an advantage over the incremental measurement in that it is not susceptible to cumulative errors.

Measured B-field approximation

In general, $\hat{B}$ can be approximated as an n order polynomial of the form:

$$\hat{B}_k(\alpha,\beta) = \sum_{i=0}^{n}\sum_{j=0}^{n} c_{ij} C_k^j S_k^i \quad (17)$$

where the subscript k denotes the k^{th} sensor; and n is the orders of the approximation. For the sensor pairs defined in (4a,b), $B_{X\pm}$ is an even function of α but odd function of β, and vice versa for $B_{Y\pm}$. Thus, C_k and S_k have the form:

$$B_{X\pm}: \quad C_1 = C_2 = \cos\alpha \text{ and } S_1 = -S_2 = \sin\beta \quad (18a)$$

$$B_{Y\pm}: \quad C_3 = C_4 = \cos\beta \text{ and } S_3 = -S_4 = \sin\alpha \quad (18b)$$

Using the least-square method, the coefficients c_{ij} in (17) can be obtained by minimizing the summed squared error

$$E_k = \sum_{i=1}^{n_i}\sum_{j=1}^{n_j}\left[B_k(\alpha_i,\beta_j) - \hat{B}_k(\alpha_i,\beta_j)\right]^2 \quad (19)$$

where $B_k(\alpha,\beta)$ is the analytical solution (3).

Solutions to the Inverse Problem

Once $\hat{B}$ is modeled, the orientation (α, β) can be obtained by solving the inverse problem; the solution depends on the order of the approximation. In general, two equations can be obtained for each of the sensor pairs:

$$\overline{B} = \frac{\hat{B}_+ + \hat{B}_-}{2} = \sum_{i=0}^{n}\left(\sum_{j=0}^{n} c_{ij} C^j\right) S^i \quad \text{where } i \text{ is even.} \quad (20a)$$

$$\tilde{B} = \frac{\hat{B}_+ - \hat{B}_-}{2} = \sum_{i=1}^{n}\left(\sum_{j=0}^{n} c_{ij} C^j\right) S^i \quad \text{where } i \text{ is odd.} \quad (20b)$$

Two independent sets of inverse solutions, $\langle\hat{\alpha}_1,\hat{\beta}_1\rangle$ and $\langle\hat{\alpha}_2,\hat{\beta}_2\rangle$, can be solved from the pair of equations; one from each sensor pair. The orientation angles are estimated as follows:

$$\begin{bmatrix}\hat{\alpha}\\ \hat{\beta}\end{bmatrix} = \mathbf{W_1}\begin{bmatrix}\hat{\alpha}_1\\ \hat{\beta}_1\end{bmatrix} + \mathbf{W}_2\begin{bmatrix}\hat{\alpha}_2\\ \hat{\beta}_2\end{bmatrix} \quad (21a)$$

where $\mathbf{W_1}$ and $\mathbf{W_2}$ are the 2×2 weighting matrices. For the sensor pair defined in (4a,b), the following matrices are chosen:

$$\mathbf{W_1} = \begin{bmatrix}1 & 0\\ 0 & 0\end{bmatrix}, \mathbf{W}_2 = \begin{bmatrix}0 & 0\\ 0 & 1\end{bmatrix} \quad (21b)$$

Illustrative Example 2

For the 1st order approximation (n=1), the inverse solutions are given by (22a, b):

$$\overline{B}_X = \left(\hat{B}_{X+} + \hat{B}_{X-}\right)/2 = c_{00} + c_{01}\cos\alpha \quad (22a)$$

$$\tilde{B}_X = \left(\hat{B}_{X+} - \hat{B}_{X-}\right)/2 = \left(c_{10} + c_{11}\cos\alpha\right)\sin\beta \quad (22b)$$

$$\overline{B}_Y = \left(\hat{B}_{Y+} + \hat{B}_{Y-}\right)/2 = c_{00} + c_{01}\cos\beta \quad (22c)$$

$$\tilde{B}_Y = \left(\hat{B}_{Y+} - \hat{B}_{Y-}\right)/2 = \left(c_{10} + c_{11}\cos\beta\right)\sin\alpha \quad (22d)$$

Two estimated solutions are obtained independently from (22a, b) and (22c,d) independently:

$$\hat{\alpha}_1 = \cos^{-1}\left[\left(\bar{B}_X - c_{00}\right)/c_{01}\right] \text{ ; and}$$

$$\hat{\beta}_1 = \sin^{-1}\left[\tilde{B}_X/\left(c_{10} + c_{11}\cos\hat{\alpha}_1\right)\right].$$

Similarly, from (21c,d),

$$\hat{\alpha}_2 = \cos^{-1}\left[\left(\bar{B}_Y - c_{00}\right)/c_{01}\right] \text{; and}$$

$$\hat{\beta}_2 = \sin^{-1}\left[\tilde{B}_Y/\left(c_{10} + c_{11}\cos\hat{\alpha}_2\right)\right]$$

where $(\hat{B}_{Y+} + \hat{B}_{Y-})/2$.

Higher order approximations, though lengthy, can be solved similarly. In general, the inverse solutions become complex as the order increases.

RESULTS AND DISCUSSIONS

To provide some insights to the angle measurements, we simulate the performance of the sensing methods by computing the measurement errors, and compare the absolute orientation against the methods single–dipole approximation (11) and incremental measurement (16). We also simulate the effects of sensor location and orientation to provide some hints on the choice of the weighting matrices.

A. Effect of the polynomial order

We simulate the magnetic field of the two sensor-pairs defined in (4a,b). The values of the sensor system parameters used in the simulation are listed in Table 1.

Figure 2(a) graphs the analytical solutions of the magnetic field B_Y at the point P(0, S, Z_s) computed using (3) over a (α, β) range of ±20°, for which the simulated measurements of constant $B_{X\pm}$ and $B_{Y\pm}$ contours (in Tesla) are plotted in Fig. 2(b). Since the sensors are placed symmetrically about the x and y axes, only one sensing quadrant is presented. As expected, the contours are circular in nature and the sensor readings decrease as the PM moves towards the center.

Table 1 Simulation Parameters

Magnet: $\lvert\mathbf{M}\rvert = M\mathbf{e}_z$ **,** M=1.35T, a=0.25inch, L=0.5inch	**Dipole parameters** (k=1,n=6); δ=0.5136 m_o=-0.229; m_{1i}=0.618 Model error = 1%

Sensor location/orientation: S=0.85inch, Z_s=1.25inch
Measured magnetic flux: $\mathbf{s}_{1\pm} = \pm B_x\,\mathbf{e_x}$; $\mathbf{s}_{2\pm} = \pm B_y\,\mathbf{e_y}$

For the sensor pairs defined in (4a,b), the coefficients in (17) are computed using Matlab Optimization toolbox minimizing the error (18); the results of three different orders of approximation are given in Table 2. Figures 3(a), 3(b) and 3(c) compare the magnetic field densities and errors approximated using 1st, 2nd and 3rd orders respectively.

As shown in Fig. 3(a), the 1st order approximation, which is linear in α and β, relatively poor in capturing sharp changes. The maximum error, however, can be reduced by increasing the order of the approximation as compared in Table 2. With the 3rd order approximation, the maximum error can be kept within 1% as shown in Fig. 3(c) where the errors are relatively uniform over the measured range.

Table 2 Coefficients for approximation

c_{ij}	1st	2nd	3rd
c_{00}	-0.3187	0.2440	13.0731
c_{01}	0.3439	-0.6157	-40.2560
c_{02}		0.3984	41.2166
c_{03}			-14.0072
c_{10}	1.5028	-24.63	-39.7679
c_{11}	-1.6099	52.1366	117.58
c_{12}		-27.6219	-114.792
c_{13}			36.89
c_{20}		92.9403	-1733.83
c_{21}		-195.3960	5449.07
c_{22}		102.7010	-5709.5
c_{23}			1994.51
c_{30}			5812.28
c_{31}			-18211.4
c_{32}			19019.7
c_{33}			-6621.01
Max. error	17.6%	8.3%	0.9%

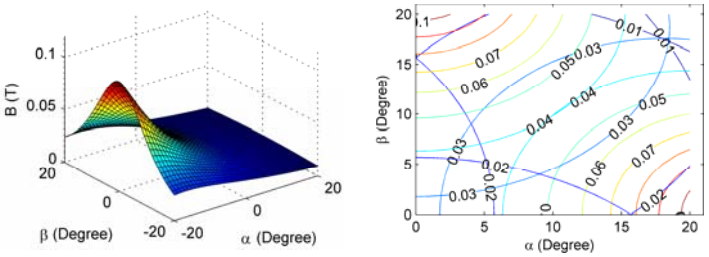

(a) Analytical solution (b) Simulated B_{x+} and B_{y+}

Fig. 2 Exact solutions and simulated measuements

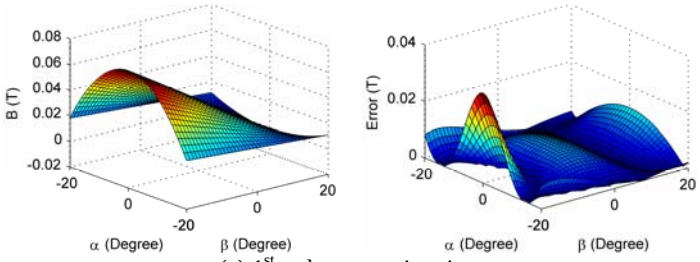

(a) 1st order approximation

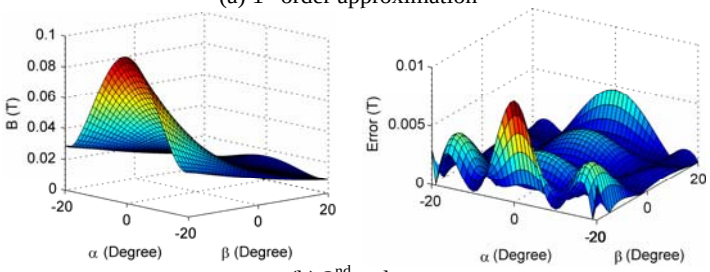

(b) 2nd order

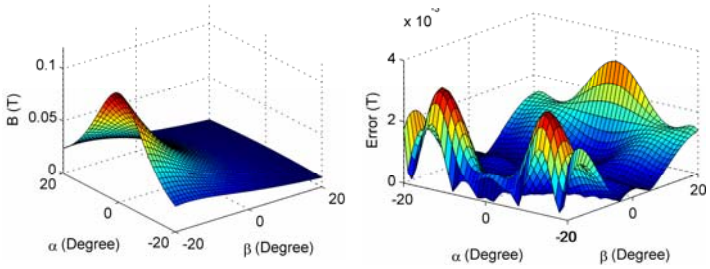

(c) 3rd order

Fig. 3 Approximate magnetic field density

Figure 4(a) shows the circular trajectory of the shaft inclined at 10° from the Z-axis. The measurement errors (in radians) corresponding to the three different orders (n=1, 2, 3) of the approximation are plotted in Fig. 4(b), (c) and (d). Figure 5

compares the maximum errors of the absolute orientation measurement against two other methods of approximation; single–dipole approximation (11) and incremental orientation measurement (16).

Several observations can be made from the results:

i) Single dipole approximation, which neglects the physical dimension of the magnet, offers limited accuracy as shown in Fig. 5.

ii) As compared in Fig. 5 and Table 5, the measurement errors based on polynomial approximation decrease as the order increases. For the range of ±20°, errors less than 5 μradians can be obtained with the 3rd order approximation.

iii) The errors of the incremental measurement depend on step size as shown in Fig. 6

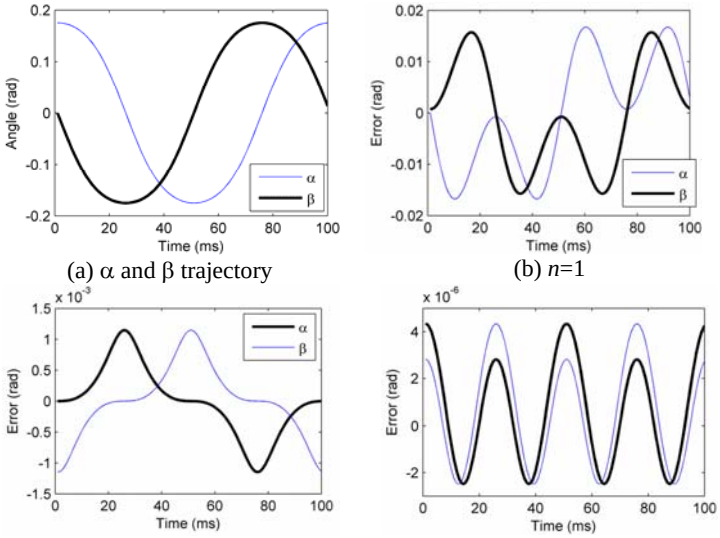

(a) α and β trajectory (b) n=1

(c) n =2 (d) n=3

Fig. 4 Absolute orientation measurement errors (10° inclination)

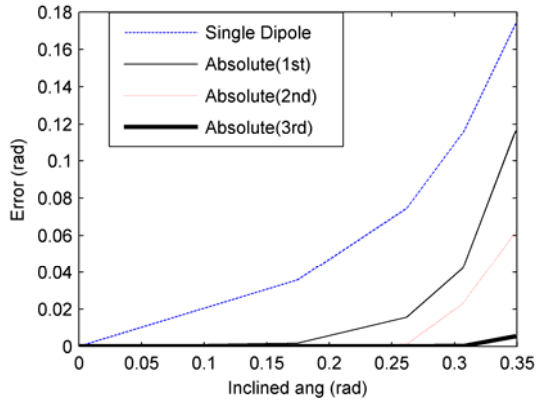

Fig. 5 comparison of maximum errors

B. Effect of Sensor Location and Orientation

The two angles (α,β) can be theoretically computed from any two of four equations. We exploit the redundancy for improving the sensor performance. To provide some insights to the choice of the weighting matrices (21b), we simulate the setup where both pairs of sensors measure the magnetic field density in the Y-direction $\hat{B}_{Y\pm}$ located on the following coordinates:

$$\mathbf{S}_{1\pm} = \begin{bmatrix} \sqrt{2}S & \pm\sqrt{2}S & Z_s \end{bmatrix}^{\mathrm{T}} \tag{23a}$$

$$\mathbf{S}_{2\pm} = \begin{bmatrix} \pm\sqrt{2}S & \sqrt{2}S & Z_s \end{bmatrix}^{\mathrm{T}} \tag{23b}$$

$$C_1 = C_2 = -C_3 = -C_4 = \sin\alpha \tag{23c}$$

$$S_1 = -S_2 = -S_3 = S_4 = \sin\beta \tag{23d}$$

Fig. 7 summarizes the results of the simulation, where the corresponding coefficients in (17) are given in Fig. 7(b). Figure 7(a) shows the exact solution of the magnetic field. Figure 7(c) graphs the magnetic field based on the 2nd order approximation and its modeling error of the magnetic field. As compared in Figs. 7(d) and 7(e), since both pairs of sensors measure the magnetic field density in the Y-direction $\hat{B}_{Y\pm}$, the β angles are measured much more accurately than the α angle.

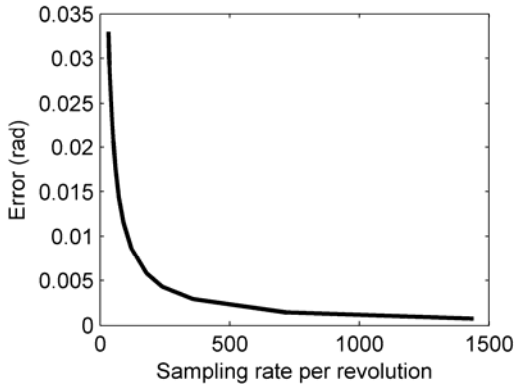

Fig. 6 Effects of sampling rate on Incremental measurement (10°inclination)

Conclusions

We derived the inverse solution of the distributed multi-pole (DMP) model for the design a magnetic field-based sensor of measuring the multi-DOF model. The DMP model extends the concept of a magnetic dipole and doublet beyond the context of physics to account for the shape and magnetization of the physical magnet. The simplicity of the closed-form solutions along with precise (and yet intuitive) magnetic fields of the DMP models have been demonstrated to show how the inverse DMP models can be efficiently characterize the magnetic fields for real-time orientation measurement.

Two different approaches, which relax the single dipole assumption to allow for a broader application of magnetic sensors for measuring the orientation of a three-DOF actuator in real time, have been derived; incremental and absolute orientation. Simulation results are given to provide insights to the performance of the sensing methods by computing and comparing the measurement errors the absolute orientation, incremental measurement, against the method based single–dipole approximation and exact solution. We show that how an inexpensive magnetic sensor (such as a Hall Effect) can be used to provide redundant measurements and to provide some insights to the choice of the weighting matrices. We also investigate by simulation the effects of sensor location and orientation.

The advantage of the magnetic sensor is that it measures the magnetic field directly, which can be used to calculate the magnetic force and torque involved. The trade-off is that it

requires the inverse solution of the magnetic field. We have shown in this paper how the inverse solution can be derived from the DMP model which is given in closed form. The ability to characterize magnetic fields and forces in addition to orientation sensing can offer a number of advantages in real-time computation and control.

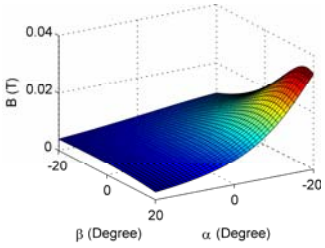

(a) Analytical solutions

c_{ij}	1st	2nd
c_{00}	0.0104	0.0099
c_{01}	-0.0254	-0.0249
c_{02}		0.0243
c_{10}	0.0104	0.0047
c_{11}	-0.0584	-0.0583
c_{12}		0.1352
c_{20}		-0.0188
c_{21}		-0.0130
c_{22}		0.1875

(b) coefficients

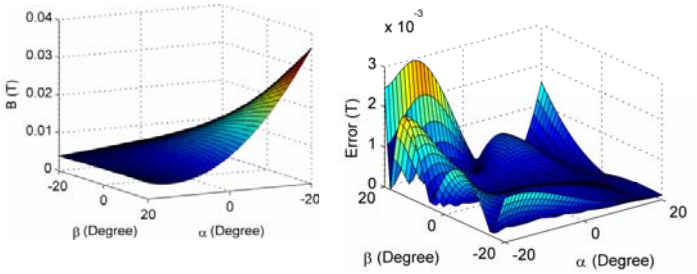

(c) 2nd order approximation of magntic field density

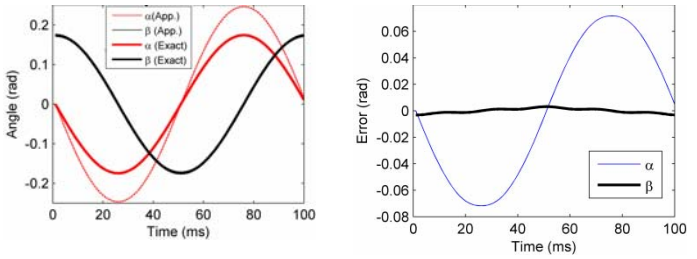

(d) Orientation angles (e) α and β measurement errors

Fig. 7 Effects of sensor locations on measurement errors

Nomenclature

Capitalized symbols		Lowercase symbols	
B	Magnetic flux density	a	Radius of PM
$\hat{B}$	Estimation of **B**	ℓ	Length of PM
E	Error of B field	k	Number of loop of DMP
H	Magnetic flux intensity	m	Dipole strength
$\mathbf{M}_o$	Magnetization vector	n	Number of poles in the loop
S	Sensor location	$\mathbf{e}_{x,y,z}$	Unit vector
S_x	sin (x)	**Greek letter symbols**	
C_x	cos(x)	α, β, γ	ZYZ Euler angles
L	Distance of PM	ε_R	Error tolerance
P	Arbitrary point at space	η, δ	Locations of PM
$\mathbf{R}_{ji\pm}$	Distance of source/sink to P	μ_o	free space permeability
W	Weighting matrix	Φ	Magnetic potential
Z_s	The height of sensor plane	Γ	Transformation matrix

ACKNOWLEDGEMENT

This project has been funded jointly by the U .S. Poultry and Eggs Association and the Georgia Agricultural Technology Research Program.

REFERENCES

[1] Clarke, W., "Mercedes-Benz F-400 Carving," edmunds.com, 2002

[2] Peter, J., "The Wave of the Future?" Automotive Industries: Wavecrest, January, 2004

[3] Lee, K-M, 1995, Orientation Sensing System and Method for a Spherical Body, U.S. Patent 5,319,577, April 25.

[4] Lee, K.-M. and R. Blenis, 1994, Design Concept and Prototype Development of a Flexible Integrated Vision System, Journal of Robotic Systems, 11(5), 387-398.

[5] Lee, K.-M. and D. Zhou," A Real-time Optical Sensor for Simultaneous Measurement of Three-DOF Motions," IEEE/ASME Transactions on Mechatronics, Vol. 9. No. 3 September 2004, pp. 499-507.

[6] Lee, K.-M. and H. Son, "Torque model for design and control of a spherical wheel motor", IEEE/ASME AIM2005 Proc. p. 335-340.

[7] Lenz, J. and A. S. Edelstein, "Magnetic Sensors and Their Applications," IEEE Sensors Journal, Vol. 6, No. 3, June 2006.

[8] Choi, S., S.-H. Kim, Y.-K. Yoon, and M. G. Allen, "A Magnetically Excited and Sensed MEMS-Based Resonant Compass," IEEE Transactions on Magnetics, Vol. 42, No. 10, October 2006.

[9] H. Son and K.-M. Lee "Distributed multi-pole model for motion simulation of PM-base spherical motor," IEEE/ASME AIM2007.

[10] Lee, K.-M. and H. Son, "Equivalent Voice-coil Models for Real-time Computation in Electromagnetic Actuation and Sensor Applications," IEEE/ASME AIM2007.

[11] Yabukami, S, H. Kikuchi, M. Yamaguchi,K. I. Arai,K. Takahashi, A. Itagaki, and N. Wako, "Motion Capture System of Magnetic Markers Using Three-Axial Magnetic Field Sensor," IEEE Transactions on Magnetics, Vol. 36, No. 5, November 2000.

[12] Paperno, E. and P. Keisar, "Three-Dimensional Magnetic Tracking of Biaxial Sensors," IEEE Transactions on Magnetics, Vol. 40, No. 3, May 2004.